

A DEEP VIEW OF THE MONOCEROS RING IN THE ANTICENTER DIRECTION: CLUES OF ITS EXTRA-GALACTIC ORIGIN

A. SOLLIMA^{1,2,3}, D. VALLS-GABAUD⁴, D. MARTINEZ-DELGADO^{5,1,2}, J. FLIRI⁴, J. PEÑARRUBIA⁶, H. HOEKSTRA^{7,8}

Draft version June 13, 2018

ABSTRACT

We present the results of deep imaging obtained at the CFHT with MegaCam in the Anticenter direction at two different heights above the Galactic disk. We detect the presence of the Monoceros ring in both fields as a conspicuous and narrow Main Sequence feature which dominates star counts over a large portion of the color-magnitude diagram down to $g' \sim 24$. The comparison of the morphology and density of this feature with a large variety of Galactic models excludes the possibility that it can be due to a flare of the Galactic disk, supporting an extra-Galactic origin for this ring-like structure.

Subject headings: Galaxy: structure — galaxies: interactions — Galaxy: disk — methods: data analysis — techniques: photometric

1. INTRODUCTION

The Monoceros ring represents one of the most controversial features among the various sub-structures discovered in the Milky Way. It was discovered as a ring-like structure spanning about 170° in longitude at a nearly constant Galactocentric distance at low-latitudes (Newberg et al. 2002; Yanny et al. 2003). Its structure and extent have been later studied by many authors using both photometric (Rocha-Pinto et al. 2003; Ibata et al. 2003; Conn et al. 2005a, 2007) and spectroscopic (Crane et al. 2003) data. On the basis of these analyses, the Monoceros (Mon) stream has been found on both sides of the plane of the Galaxy at Galactocentric distances $15 < R < 20$ kpc. Subsequent spectroscopic studies indicated that this structure is kinematically cold ($13 < \sigma_v < 20$ Km s⁻¹; Conn et al. 2005b; Martin et al. 2006; Casetti-Dinescu et al. 2008) and homogeneous in metal content ($\sigma_{[Fe/H]} \sim 0.15$ dex; Ivezić et al. 2008, hereafter I08). The nature of the Mon ring is highly debated: in fact it is not clear if this feature is a debris from an accreted satellite (e.g. Helmi et al. 2003; Martin et al. 2004; Penarrubia et al. 2005; Martinez-Delgado et al. 2005) or an intrinsic feature of the Galactic disk possibly associated to the disk flare (Momany et al. 2006, hereafter M06; Hammersley & Lopez-Corredoira 2011), the Norma-Cygnus spiral arm (Moitinho et al. 2006), perturbations due to past accretion events (Kazantzidis et al. 2008) or the second dark matter caustic ring (Natarajan & Sikivie 2007).

antonio.sollima@oapd.inaf.it

¹ Instituto de Astrofísica de Canarias, E38205 San Cristobal de La Laguna, E38205, Spain

² Departamento de Astrofísica, Universidad de La Laguna, E-38205 San Cristobal de La Laguna, Spain

³ INAF Osservatorio Astronomico di Padova, I35122 Padova, Italy

⁴ GEPI, CNRS UMR 8111, Observatoire de Paris, 92195 Meudon, France

⁵ Max Plank Institut für Astronomie, D69117 Heidelberg, Germany

⁶ Institute of Astronomy, University of Cambridge, Cambridge, CB3 0HA, United Kingdom

⁷ Department of Physics and Astronomy, University of Victoria, Victoria, BC V8P 1A1, Canada

⁸ Leiden Observatory, Leiden University, PO Box 9513, 2300 RA, Leiden, the Netherlands

In this *Letter* we present the detection of the Mon ring toward the Galactic anticenter at two different Galactic latitudes and use its color-magnitude diagrams (CMDs) to investigate the possible connection between this object and the Galactic disk flare. The Anticenter represents a particularly convenient direction to test this scenario since *i*) it lies close to the line of nodes where the effects of the Galactic warp are minimized (Drimmel & Spergel 2001), *ii*) it avoids contamination from bulge stars, and *iii*) it lies along a radial away from the Galactic center, following the direction of growth of the disk scale-height. This analysis comes from two photometric campaigns performed with MegaCam@CFHT devoted to the study of weak lensing in massive clusters of galaxies (see Hoekstra 2007) and to the search for extra-tidal structures in the outskirts of outer halo globular clusters (Martinez-Delgado et al. 2004).

2. OBSERVATIONS AND DATA REDUCTION

The photometric data have been obtained with the MegaCam camera, mounted at the Canada-France-Hawaii Telescope (CFHT)(Mauna Kea, Hawaii). The camera consists of a mosaic of 36 chips with a pixel scale of $0.185'' \text{ pixel}^{-1}$ providing a global field of view of $\sim 1^\circ \times 1^\circ$. Observations have been performed in Service Mode in two different observing runs on October 2005 (3 nights) and January 2009 (two nights). The two datasets consists in a set of 15 (4 g' and 11 r') 600 sec-long and 13 (6 g' and 7 r') 680 sec-long images centered at $(\alpha, \delta) = (7h 18m 08s, +37^\circ 37' 45'')$ (field 1) and $(\alpha, \delta) = (7h 38m 08s, +38^\circ 54' 00'')$ (field 2) with a dithering pattern of few arcminutes to fill the gaps between the chips. The average seeing for the two datasets was $0.7''$ and $1.0''$, respectively.

The standard reduction steps (bias, dark and flat-field correction) have been performed using the Elixir pipeline developed by the CFHT team. We used DAOPHOT II and the PSF fitting algorithm ALLSTAR (Stetson, 1987) to obtain instrumental magnitudes for all the stars detected in each frame. Mean frames have been obtained by aligning and averaging all the g' and r' images with a 3 σ clipping rejection threshold, using the Terapix⁹ software

⁹ <http://terapix.iap.fr>

specifically devoted to this task. The automatic detection of sources has been performed on the mean frame adopting a 3σ threshold. The file with the object positions has been then used as input for the PSF-fitting procedure, that has been performed independently on each image. As usual, the most isolated and bright stars in each field have been employed to build the PSF model (here a Moffat function of exponent 2.5 has been adopted). For each passband, the derived magnitudes have been transformed into the same instrumental scale and averaged. We adopted the nightly zero points and reddening coefficients provided by the CFHT team to link the instrumental magnitudes to the standard system. Finally, a catalog with more than 40,000 calibrated sources has been produced. The photometrically calibrated catalog has been cross-correlated with the seventh data release of the Sloan Digital Sky Survey (SDSS; Abazajian et al. 2009) catalog, which lists accurate positions for more than 3,000 objects over an area of π sq.deg. around both fields, to derive an accurate astrometric solution with a typical r.m.s of 200 mas. These catalogs represent the deepest and most accurate datasets on the Mon feature, with over 3 times more stars and a photometric accuracy about an order of magnitude better than previous SDSS data.

3. RESULTS

3.1. Color-Magnitude Diagrams

In Fig. 1 the $g' - r'$, g' CMDs of the two fields are shown. Only objects with a sharpness parameter $|S| < 0.5$ (as defined by Stetson 1987) have been plotted to avoid contamination from background galaxies. As can be noted, the CMDs sample the foreground Galactic population, reaching a limiting magnitude $g' \sim 25.5$. A significant overdensity of stars can be noticed in both fields at $g' - r' < 1$ and $19 < g' < 24$, with a morphology which resembles a Main Sequence (MS). It is evident from Fig. 1 that the density of MS stars is significantly smaller in field 2 compared with field 1.

The present detections are located close to the region where the Mon ring was discovered (Newberg et al. 2002). More recently, Grillmair (2006) found a compact overdensity of stars above the background field population at an height of ~ 30 degrees above the Galactic plane close to the previous detection of Mon (the "Anticenter stream"). Although the possible association between the Anticenter stream and Mon is still debated (see Carlin et al. 2010 and references therein), our target fields are located at lower Galactic latitudes ($\Delta b \sim 12^\circ$) with respect to the Anticenter stream overdensity, being therefore unrelated with such structure.

3.2. Synthetic CMDs

To test the possible association of the MS feature observed in Fig. 1 with the disk flare we simulated a series of synthetic CMDs for the Galactic field population following the prescription of seven different Galactic models: Drimmel & Spergel (2001; hereafter DS01); Lopez-Corredoira et al. (2002; L02); Robin et al. (2003; R03), Foster & Routledge (2003; FR03), Yusifov (2004; Y04), Hammersley & Lopez-Corredoira (2010; HL11) and a simple model which has been calibrated to fit the 2MASS data of the disk flare and warp collected by M06. Hereafter, we will refer to this best-fit model as S11. For this

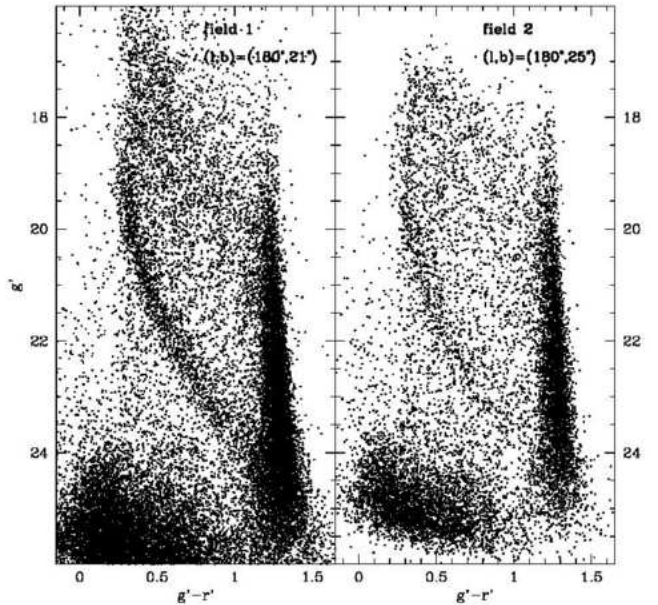


FIG. 1.— CMDs of field 1 (left panel) and field 2 (right panel). Only stars with a sharpness parameter $|S| < 0.5$ are plotted. The clump visible at $g' > 24$, $g' - r' < 0.5$ is due to the contamination of unresolved background galaxies.

TABLE 1
BEST-FIT PARAMETERS OF THE BEST-FIT S11 MODEL

Parameter	Value	Description
R_\odot	8.5 kpc	Solar Galactocentric distance
Z_\odot	15 pc	Solar height above the Galactic plane
q	0.63	Halo flatness parameter
f	0.9	Fraction of thin disk stars
f_h	0.001	Fraction of halo stars
n_h	2.77	Halo density power-law coefficient
R_1	1.99 kpc	Thin disk scale-length
R_2	2.99 kpc	Thick disk scale-length
$h_{Z,1}(R_\odot)$	193 pc	Thin disk scale-height at the Solar circle
$h_{Z,2}(R_\odot)$	611 pc	Thick disk scale-height at the Solar circle
h_{fl}	23.0 kpc	Flare characteristic radius
Z_0	370 pc	Maximum warp height
R_w	11.5 kpc	Warp starting radius
h_w	3.0 kpc	Warp characteristic radius
ϕ_0	11°	Line of nodes angle

last model we adopted an oblate spheroidal halo with a declining profile of the form

$$\rho_h(R, Z) = f_h \rho_{\odot,d} \left(R_\odot / \sqrt{R^2 + (Z/q)^2} \right)^{n_h} \quad (1)$$

The disk has been modelled as a sum of two exponential disks (Juric et al. 2008; hereafter J08)

$$\rho_d(R, Z) = \rho_{\odot,d} \left(f e^{-(R-R_\odot)/R_1 - (Z+Z_\odot)/h_{Z,1}} + (1-f) e^{-(R-R_\odot)/R_2 - (Z+Z_\odot)/h_{Z,2}} \right) \quad (2)$$

The scale-heights of both disks have been assumed to increase with distance from the Galactic center to take into account the disk flare

$$h_{Z,i}(R) = h_{Z,i}(R_\odot) e^{(R-R_\odot)/h_{fl}} \quad (3)$$

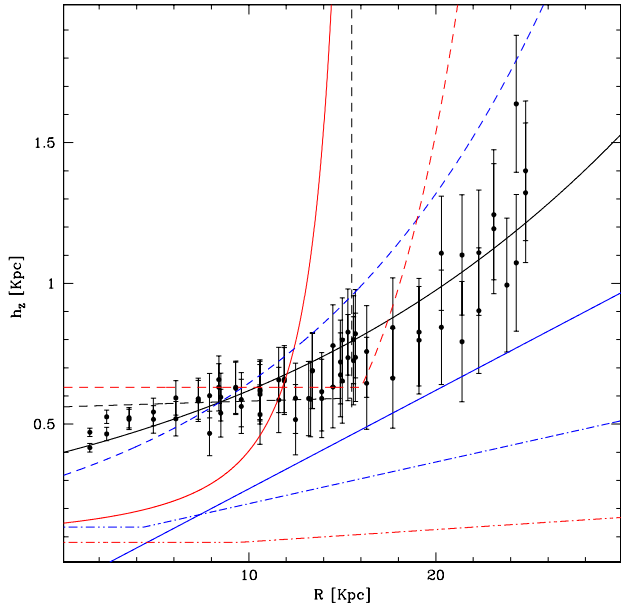


FIG. 2.— Disk scale-height as a function of the Galactocentric distance. The measures by M06 are plotted as filled circles. The prediction of the various models (DS01: blue dot-dashed line; L02: red solid line; R03: red dot-dashed line; FR03: blue solid line; Y04: blue dashed line; S11: black solid line; HL11: red dashed line; "wall flare" model: black dashed line) are overplotted.

Finally, the disk warp has been modelled as a series of tilted rings whose disk heights is defined as

$$Z_w(Z, \phi) = Z_0 \tanh((R - R_w)/h_w) \sin(\phi - \phi_0) \quad \text{for } R > R_w \quad (4)$$

where ϕ is the angle with respect to the Sun direction in a cylindrical system of coordinates centered on the Galactic center. In the definition of our best-fit model we kept fixed those parameters derived by J08 and left free the 4 ones which determine the warp and flare shape (h_{fl} , Z_0 , h_w and ϕ_0). The final values of all the parameters involved in the above model are listed in Table 1. The value of $\rho_{\odot,d}$ has been normalized to reproduce the observed number of stars in field 1.

All the above models take into account for both the disk flare and warp and have been calibrated to reproduce the density of different markers: warm dust (DS01), bright stars (L02), dwarf stars (R03, HL11), HI gas (FR03), pulsars (Y04) and red clump stars (M06). In Fig. 2 the prediction of the various models considered in this work are compared with the data collected by M06. Note that significant differences are evident between the various models mainly resulting from the different objects used as disk markers.

The overall CMD has been simulated as the sum of the contribution of the halo and disk stellar populations. We ignored the bulge contribution assuming it negligible in the Anticenter direction. For each Galactic component we randomly extracted a population of stars from a Kroupa (2001) mass function with suitable ages and metallicities¹⁰. Only R03 and HL11 distinguish between

thin and thick disk adopting two different characteristic lengths and heights. For the other models we simulated the Galactic disk population as a mixture of thin and thick disk stars in proportions established by J08. This approximation ensures a good level of accuracy in reproducing the CMD (see also DS01; L02; FR03; M06; Reyle et al. 2009). We adopted a two-step star formation rate (SFR) and the age-metallicity relation from Fuhrmann (1998) for the thin disk (Girardi et al. 2005), while for the thick disk a constant SFR between 11 and 12 Gyr and a gaussian metallicity distribution with $[M/H] = -0.4 \pm 0.1$ has been assumed (Girardi et al. 2005). For the halo, we assumed a constant SFR between 12 and 13 Gyr and the metallicity distribution derived by Ryan & Norris (1991). A fraction of binaries of $f = 50\%$ (Duquennoy & Mayor 1991) has been simulated by randomly associating pairs of stars and calculating the corresponding magnitudes by summing the fluxes of the two components (see Rubenstein & Bailyn 1997). Absolute magnitudes and dereddened colors have been then derived using the evolutionary tracks by Marigo et al. (2008) in the MegaCam photometric system. Halo and disk stars have been then located at different distances according to the prescription of each Galaxy model. For each star a proper extinction has been included by calculating the dust column density at the star's distance assuming a dust distribution across the disk of the form $\rho_{dust} \propto e^{-R/R_{dust}} \text{sech}^2(Z/Z_{dust})$ with a scale-height of $Z_{dust} = 134.4$ pc and a scale-length of $R_{dust} = 2.26$ kpc (DS01), and normalized by imposing the extinction at infinity predicted by the Schlegel et al. (1998) maps. The distance and extinction have been finally used to convert absolute magnitudes and colors into apparent ones. Photometric errors and incompleteness have been estimated by means of artificial stars experiments which have been performed on the CFHT images. A detailed description of the adopted procedure can be found in Bellazzini et al. (2002).

In Fig 3 the observed CMD of field 1 and the corresponding synthetic CMDs are shown. It is evident that while models DS01, R03, FR03 and S11 well reproduce the overall morphology of the Galactic field evolutionary sequences, none of them is able to reproduce the prominent MS feature clearly visible in the observed CMD. A poor representation of both the overall CMD and the Mon MS is instead given by Y04 and HL11 models. Only model L02 predicts a compact distribution of stars resembling a MS. Such an increase is due to the extreme flaring of the disk adopted by L02 (see Fig. 2) which produces a sudden increase of the density at a well defined Galactocentric distance ($R \sim 14$ kpc), while the double-exponential density law ($\rho_d \propto e^{-R/h_R - Z/h_Z}$) dampen the distribution of stars at longer distances. Note however that this model (which has been extrapolated here outside its range of validity; $R < 15$ kpc) fails to reproduce the magnitude spread of the observed MS feature as well as the morphology of both the red (at $g' < 18.5$, $g' - r' < 0.7$) and blue (at $g' - r' > 1$) field dwarfs in Fig. 1.

Summarizing, it seems impossible to reproduce the observed morphology of the CMDs with the existing models

¹⁰ Being the simulated CMDs mainly constituted by unevolved stars, they are not affected by the uncertainties on the adopted SFR for the various Galactic components, but mainly on their metal-

licity distributions, which are well constrained by spectroscopic observations (Venn et al. 2004).

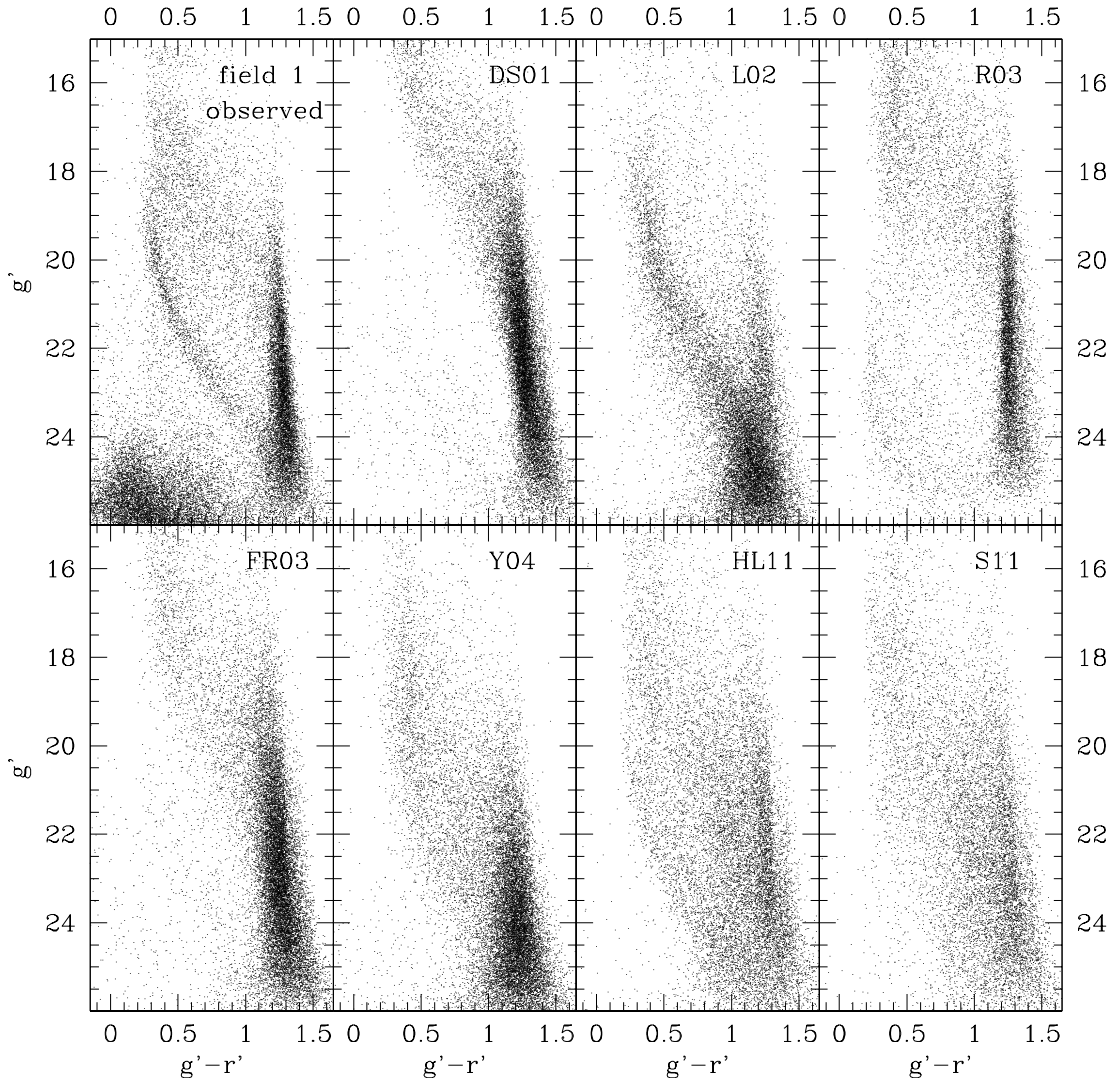


FIG. 3.— Comparison between the CMDs of field 1 and the seven Galactic models considered in this work.

of disk flare. To check the general validity of such conclusion we compared the observed CMD with a model where the most extreme disk flaring has been assumed. For this purpose we replaced in model S11 the functional form of the disks flaring (eq. 3) with a "wall" function where the scale-height of the two disks abruptly goes to infinity at a given Galactocentric distance (set to 15.5 kpc to fit the mean magnitude of the Mon MS; see Fig. 2). The simulated CMD for this model (hereafter referred as "wall flare") is shown in the central panel of Fig. 4. In Fig. 4 we compared the distribution of magnitude differences about the MS ridge line in the color interval $0.4 < g' - r' < 0.9$. It is apparent that the "wall flare" model predicts a width of the MS which is not compatible with the observed one: the standard deviation of the distribution is $\sigma_{\Delta g'} = 0.30 \pm 0.03$ in the observed CMD and $\sigma_{\Delta g'} = 0.85 \pm 0.08$ in the "wall flare" model (i.e. ~ 3 times larger). Only an "ad hoc" abrupt cutoff of the density profile of both disks at a distance close to the flare radius (in contrast with what found by

J08) would reduce the magnitude spread of this model. A second test has been performed by comparing the ratio between the number of MS stars observed in field 1 and 2 with the model prediction. For this purpose, we defined a region in the CMD containing all stars with g' magnitude within 0.5 mag about the MS ridge line defined in field 1, a color $0.4 < g' - r' < 0.9$ and a magnitude $g' < 23.8$, to avoid contamination from Galactic dwarf stars and to ensure a level of completeness $\psi > 90\%$ in both fields. While the fraction of MS stars appears to increase by a factor $N_1/N_2 = 1.87 \pm 0.11$, the "wall flare" model predicts a small decrease of this fraction ($N_1/N_2 = 0.92 \pm 0.03$)¹¹. Therefore, on the basis of the above analysis we conclude that even the most extremely

¹¹ The N_1/N_2 population ratio calculated in the "wall flare" model turns out to be smaller than unity since the small shift in magnitude produced by the decrease of latitude moves part of the MS feature outside the adopted selection box. This is a consequence of the large magnitude spread of the MS feature predicted by this model.

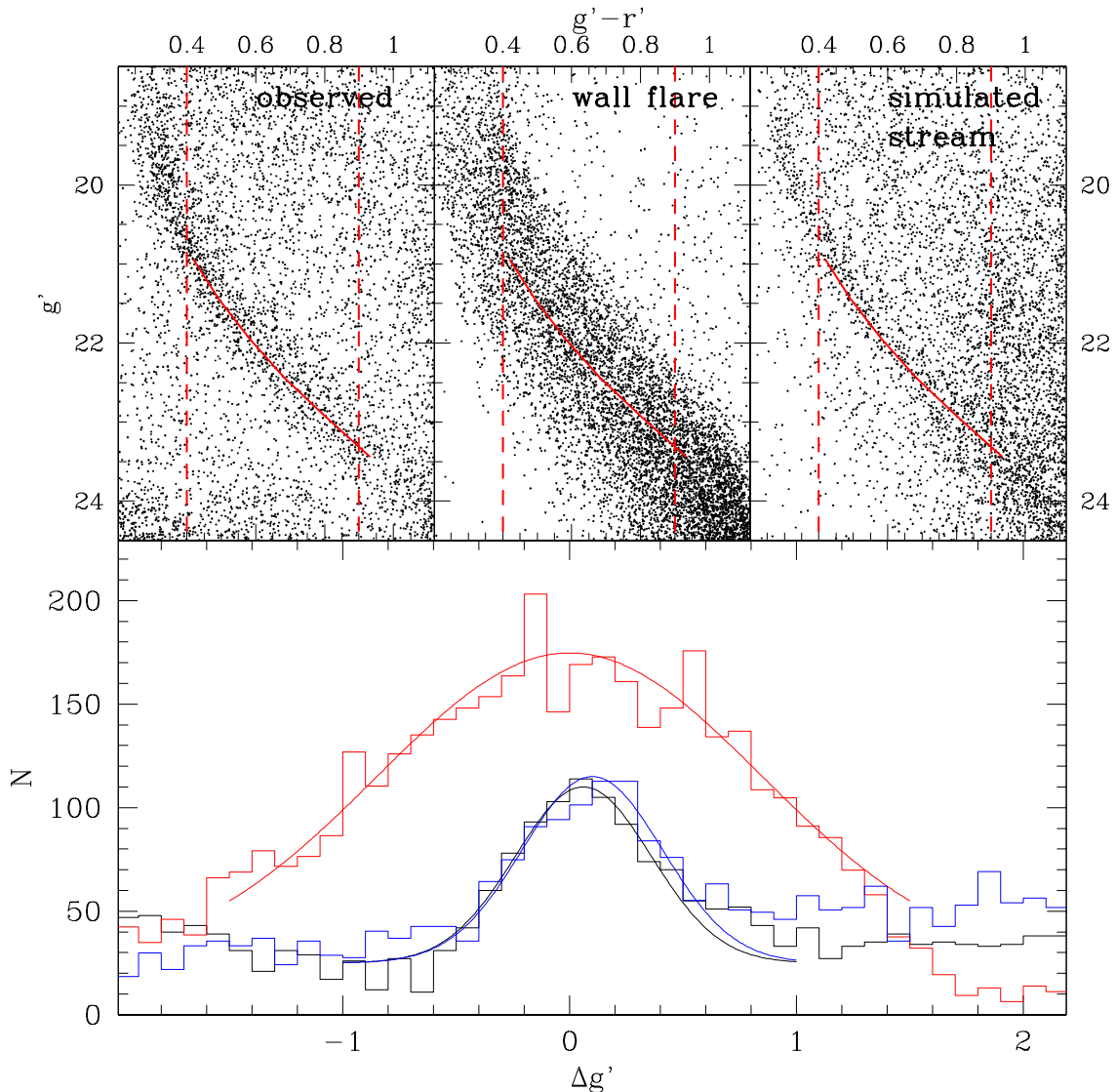


FIG. 4.— Upper panels: Zoomed CMDs of field 1 (upper-left panel), “wall flare” model (upper-central panel) and simulated stream model (upper-right panel). The MS ridge line and the color range used to construct the magnitude distribution are shown with red solid and dashed lines, respectively. Bottom panel: Distribution of magnitude differences about the MS ridge line for the observed CMD of field 1 (black histograms), “wall flare” model (red histograms) and the simulation for a discrete stream (blue histograms). The best-fit gaussians are overplotted.

acceptable flared disk model cannot reproduce the observed CMD since it fails to predict: *i*) the population of both blue and red field dwarfs; *ii*) the 2MASS data of the flare measured by M06 (see Fig.2), *iii*) the magnitude dispersion of the observed MS feature, and *iv*) the ratio of MS stars at the two observed Galactic latitudes.

For comparison with the stream scenario, we constructed the synthetic CMD of a galaxy remnant located at a given distance to the Sun with a variable thickness. For this purpose, we apply the Bayesian formalism developed by Hernandez & Valls-Gabaud (2008) to infer the posterior probability distribution functions of distance and age, using as priors a gaussian function for metallicity, centred on $[Fe/H] = -0.95$ and with dispersion 0.15 (I08). We obtain maxima in the marginalised posterior probability distribution functions at an age of $t = 9.2 \pm 0.2$ Gyr and a distance of $d = 9.1 \pm 0.2$ kpc

with a dispersion of $\sigma_d = 0.90 \pm 0.08$ kpc, consistent with previous estimates for the Mon stream (Newberg et al. 2002) and the predictions of Penarrubia et al. (2005). The obtained CMD is shown in the right panel of Fig. 4. In this last case the agreement with the observed CMD is striking. A good agreement can be also found by assuming the Mon ring formed by stars with the same age and metallicity distribution of the Galactic disk (e.g. the case of a disk perturbation or a spiral arm). In this case, the best-fit distance and dispersion turn out to be $d = 12.6 \pm 0.8$ kpc and $\sigma_d = 0.3 \pm 0.2$ kpc, respectively. However, it is worth noting that while agreement can be had over the limited magnitude range used for estimating distance, the metallicity estimates by I08 argue against this scenario.

In this *Letter* we present the results of a deep MegaCam imaging of two regions in the Galactic Anticenter direction where the presence of the Mon ring is clearly evident. The high quality of our CMDs allowed to compare the morphology of the observed MS feature with the predictions of the most recent Galactic models including the effect of disk flare and warp. We find that none of the considered models is able to reproduce the position and morphology of the Mon MS or the ratio between the number of MS stars in the two observed fields, even with extreme flares. We therefore conclude that, in the absence of an "ad hoc" abrupt disk cutoff, *the photometric signature of the Mon ring cannot be explained by any smooth variation of the Galactic disk structure*. This result is in contrast with the conclusion drawn by HL11. The reason of such a discrepancy stems from the method used by these authors to calculate the predicted star counts of their model: indeed, they adopted a delta function in magnitude to calculate the number of stars displaced at a given distance to the observer neglecting many important factors like the slope of MS stars in the CMD, the composite stellar population of the Galactic components and the photometric errors that all contribute to increase the magnitude spread of MS stars. By neglecting these effects HL11 interpreted the overall magnitude spread of the Mon MS as entirely due to a distance spread, overestimating its actual dispersion.

Of course, in absence of direct spectroscopic data, our data cannot exclude the other possible interpretations of the Mon ring as the result of small scale perturbations of the Galactic disk due to various possible physical processes (see e.g. Moitinho et al. 2006; Natarajan & Sikivie 2007; Kazantzidis et al. 2008). However, our CMDs impose strong constraints on the vertical structure and extent of such a structure. Indeed, if we assume the Mon ring formed by Galactic disk stars, the location in

the CMD of the observed MS feature and its dispersion in magnitude are compatible with an object located at a distance $d = 12.6 \pm 0.8 \text{ kpc}$ to the Sun and a width of $FWHM < 1 \text{ kpc}$. This corresponds to a very compact structure located at an height above the Galactic plane of $Z \sim 4.5 \text{ kpc}$ (i.e. ~ 4.5 times the local scale-height of the disk). Moreover, the density of Mon stars decreases of almost a factor of two by moving only 4° toward higher Galactic latitudes (see Sect. 3.2). On the other hand, under the assumption that the Mon ring is due to an accretion event which occurred in a past epoch, the derived distance of $d = 9.1 \pm 0.2 \text{ kpc}$ and dispersion $\sigma_d = 0.90 \pm 0.08 \text{ kpc}$ ($FWHM = 2.1 \pm 0.2 \text{ kpc}$) are in good agreement with the prediction of the model by Penarrubia et al. (2005; see their Fig. 7).

Our results lend support to the previous studies on the metallicity distribution (I08), abundance patterns anomalies (Chou et al. 2010) and kinematics (Casetti-Dinescu et al. 2008) of this object which show that the stellar composition of the Mon ring is different from that of the Milky Way, favouring the extra-Galactic scenario. An accurate high-resolution spectroscopic survey of these faint MS stars would definitively clarify the real nature of the Mon ring.

Based on observations obtained with MegaCam, a joint project of CFHT and CEA/DAPNIA, at the CFHT observing programs 05BC19 and 09AF03. This work is based on data products produced at TERAPIX and the Canadian Astronomy Data Centre. This research was supported by the Spanish Ministry of Science and Innovation (AYA2007-65090), by ANR POMME (ANR 09-BLAN-0228) and CNRS/MAE PICASSO. We warmly thank the anonymous referee and M. Lopez-Corredoira for their helpful suggestions and Y. Momany for providing his data.

Facilities: CFHT.

REFERENCES

- Abazajian, K. N., et al. 2009, ApJS, 182, 543
 Bellazzini, M., Fusi Pecci, F., Messineo, M., Monaco, L., & Rood, R. T. 2002, AJ, 123, 1509
 Carlin, J. L., Casetti-Dinescu, D. I., Grillmair, C. J., Majewski, S. R., & Girard, T. M. 2010, ApJ, in press, arXiv:1010.5257
 Casetti-Dinescu, D. I., Carlin, J. L., Girard, T. M., Majewski, S. R., Peñarrubia, J., & Patterson, R. J. 2008, AJ, 135, 2013
 Chou, M. Y., Majewski, S. R., Cunha, K., Smith, V. V., Patterson, R. J., & Martinez-Delgado, D. 2010, ApJ, in press, ArXiv 1007.1056
 Conn, B. C., Lewis, G. F., Irwin, M. J., Ibata, R. A., Ferguson, A. M. N., Tanvir, N., & Irwin, J. M. 2005a, MNRAS, 362, 475
 Conn, B. C., Martin, N. F., Lewis, G. F., Ibata, R. A., Bellazzini, M., & Irwin, M. J. 2005b, MNRAS, 364, L13
 Conn, B. C., et al. 2007, MNRAS, 376, 939
 Crane, J. D., Majewski, S. R., Rocha-Pinto, H. J., Frinchaboy, P. M., Skrutskie, M. F., & Law, D. R. 2003, ApJ, 594, L119
 Drimmel, R., & Spergel, D. N. 2001, ApJ, 556, 181
 Duquennoy, A., & Mayor, M. 1991, A&A, 248, 485
 Foster, T., & Routledge, D. 2003, ApJ, 598, 1005
 Fuhrmann, K. 1998, A&A, 338, 161
 Girardi, L., Groenewegen, M. A. T., Hatziminaoglou, E., & da Costa, L. 2005, A&A, 436, 895
 Grillmair, C. J. 2006, ApJ, 651, L29
 Hammersley, P. L., & López-Corredoira, M. 2011, A&A, 527, A6
 Helmi, A., White, S. D. M., & Springel, V. 2003, MNRAS, 339, 834
 Hernandez, X. & Valls-Gabaud, D. 2008, MNRAS, 383, 1603
 Hoekstra, H. 2007, MNRAS, 379, 317
 Ibata, R. A., Irwin, M. J., Lewis, G. F., Ferguson, A. M. N., & Tanvir, N. 2003, MNRAS, 340, L21
 Ivezić, Ž., et al. 2008, ApJ, 684, 287
 Jurić, M., et al. 2008, ApJ, 673, 864
 Kazantzidis, S., Bullock, J. S., Zentner, A. R., Kravtsov, A. V., & Moustakas, L. A. 2008, ApJ, 688, 254
 Kroupa, P. 2001, MNRAS, 322, 231
 López-Corredoira, M., Cabrera-Lavers, A., Garzón, F., & Hammersley, P. L. 2002, A&A, 394, 883
 Marigo, P., Girardi, L., Bressan, A., Groenewegen, M. A. T., Silva, L., & Granato, G. L. 2008, A&A, 482, 883
 Martin, N. F., Irwin, M. J., Ibata, R. A., Conn, B. C., Lewis, G. F., Bellazzini, M., Chapman, S., & Tanvir, N. 2006, MNRAS, 367, L69
 Martin, N. F., Ibata, R. A., Bellazzini, M., Irwin, M. J., Lewis, G. F., & Dehnen, W. 2004, MNRAS, 348, 12
 Martínez-Delgado, D., Butler, D. J., Rix, H.-W., Franco, V. I., Peñarrubia, J., Alfaro, E. J., & Dinescu, D. I. 2005, ApJ, 633, 205
 Martínez Delgado, D., Dinescu, D. I., Zinn, R., Tutsoff, A., Côté, P., & Boyarchuck, A. 2004, Satellites and Tidal Streams, 327, 255
 Moitinho, A., Vázquez, R. A., Carraro, G., Baume, G., Giorgi, E. E., & Lyra, W. 2006, MNRAS, 368, L77
 Momany, Y., Zaggia, S., Gilmore, G., Piotto, G., Carraro, G., Bedin, L. R., & de Angeli, F. 2006, A&A, 451, 515
 Natarajan, A., & Sikivie, P. 2007, Phys. Rev. D, 76, 023505

- Newberg, H. J., et al. 2002, ApJ, 569, 245
Peñarrubia, J., et al. 2005, ApJ, 626, 128
Reylé, C., Marshall, D. J., Robin, A. C., & Schultheisé, M. 2009, A&A, 495, 819
Robin, A. C., Reylé, C., Derrière, S., & Picaud, S. 2003, A&A, 409, 523
Rocha-Pinto, H. J., Majewski, S. R., Skrutskie, M. F., & Crane, J. D. 2003, ApJ, 594, L115
Rubenstein, E. P., & Baily, C. D. 1997, ApJ, 474, 701
Ryan, S. G., & Norris, J. E. 1991, AJ, 101, 1865
Schlegel, D. J., Finkbeiner, D. P., & Davis, M. 1998, ApJ, 500, 525
Stetson, P. B. 1987, PASP, 99, 191
Venn, K. A., Irwin, M., Shetrone, M. D., Tout, C. A., Hill, V., & Tolstoy, E. 2004, AJ, 128, 1177
Yanny, B., et al. 2003, ApJ, 588, 824
Yusifov, I. 2004, The Magnetized Interstellar Medium, 165